NAFEMS World Congress 2025 – Contribution of the Virtual Validation in the development of a 48V electric powertrain for 2-wheeler applications.

M. Caggiano
(Piaggio & C. SpA, Italy);

A. Fricassè
(Piaggio & C. SpA, Italy);

R. Testi
(Piaggio & C. SpA, Italy);

Abstract

A CAE workflow was defined within a new Piaggio development methodology and executed to develop and assess the new Piaggio 48V electric powertrain's performance. The workflow involved linked CFD, EMAG and structural analyses. The objective was to anticipate fundamental results and info and reduce the economic effort associated with the physical prototyping activities. Diverse CAE suites were coupled, optimizing using Piaggio's procedures which were consolidated throughout the years for the of development of 2-wheelers equipped with internal combustion engines. The modular structure of those suites made in easier to incorporate the new EMAG analyses in the workflow. The MBS system simulation activities were carried out integrating the new E-powertrain models in a Piaggio's database, which includes libraries of subsystems such as transmissions, testbenches, etc. This approach will allow for quicker generation of future models leveraging carry-out made possible by the modular nature of such a database. The whole CAE workflow relied on a common source of truth residing in Piaggio's PLM system, allowing a smooth cooperation between Piaggio's E-Mobility and Powertrain depts. EMAG simulations were carried to assess the electric machine's performance and to provide input data for the subsequent CFD, MBS and structural analyses. The dynamic behavior, from a mechanical standpoint, was analyzed with multibody models, which produced KPIs' values and provided input data for stress analyses. CFD analyses were used to verify that the exercise temperatures were compatible with the electric machine's requirements and provided thermal maps for the FEM stress analyses. The structural integrity of the whole e-powertrain system was verified with combined stress and durability analyses, based on the working conditions identified during the previous EMAG, MBS and CFD campaigns. The structural FEM analyses were also used without coupling them with durability tools, to investigate functional aspects of the mechanical system. Being the CAE campaign carried out in the project's early

stages, it allowed to reduce the physical tests and could assist the sourcing activities managed by the Purchasing dept

1. Object of the study

Piaggio planned to develop an electric powertrain, relying on internal know-how for the design phase. A range of Piaggio vehicles, already available with ICE-based powertrains, will be commercialized in the electric version too, equipping them with the powertrain whose study is the object of the present paper.

To reduce as much as possible the trail-and-error, expensive physical test phase, massive usage of virtual engineering tools was scheduled with a final, limited set of physical tests only on the best configurations singled out with the virtual replica.

Given the product's nature, multiple disciplines were involved in the CAE workflow, including CFD, EMAG, multibody, thermos-structural FEM and durability modelling. Data were exchanged between different models via direct interfaces or external files. The geometrical metadata came from the company's main PLM/CAD system.

2. Modelling remarks

The powertrain system consists of the e-motor proper and of the gear transmission system which connects the e-motor to the vehicle's rear wheel. The CAE campaign covered the whole powertrain system and had the following objectives.

- Predict the e-motor performance via EMAG simulations.
- Verify the e-motor components structural soundness via chained CFD-FEM-durability simulations. In particular, the e-motor main shaft subsystem and the e-motor cover were analysed.

The following figures respectively show the workflows for the analysis of the main shaft and of the cover.

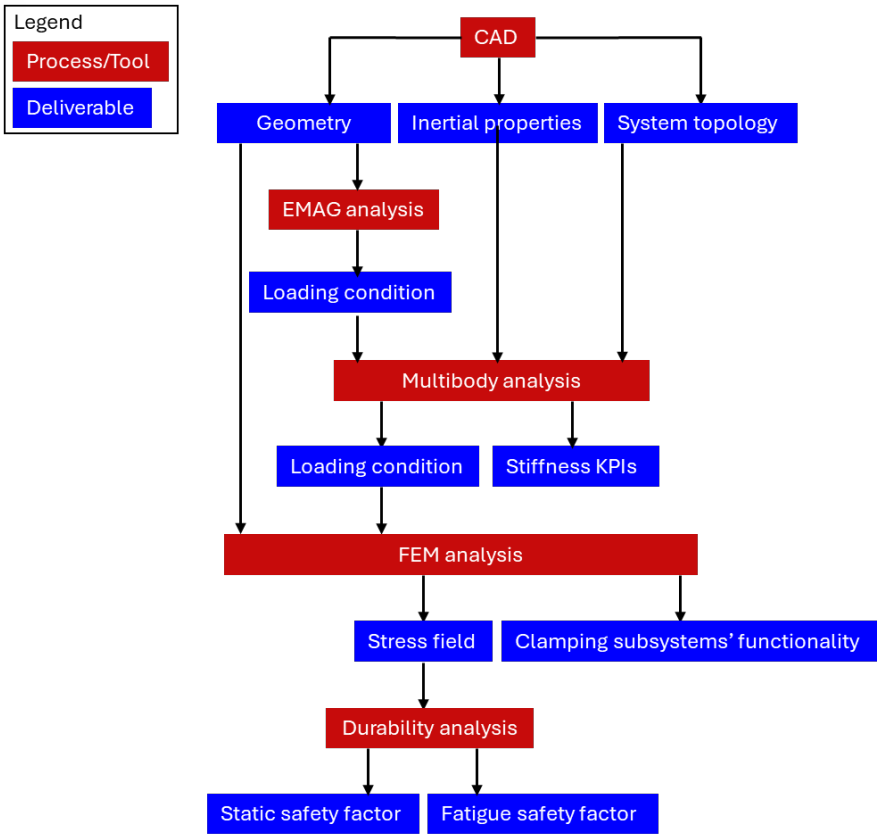

Figure 1: Modelling remarks. E-motor's main shaft. CAE workflow.

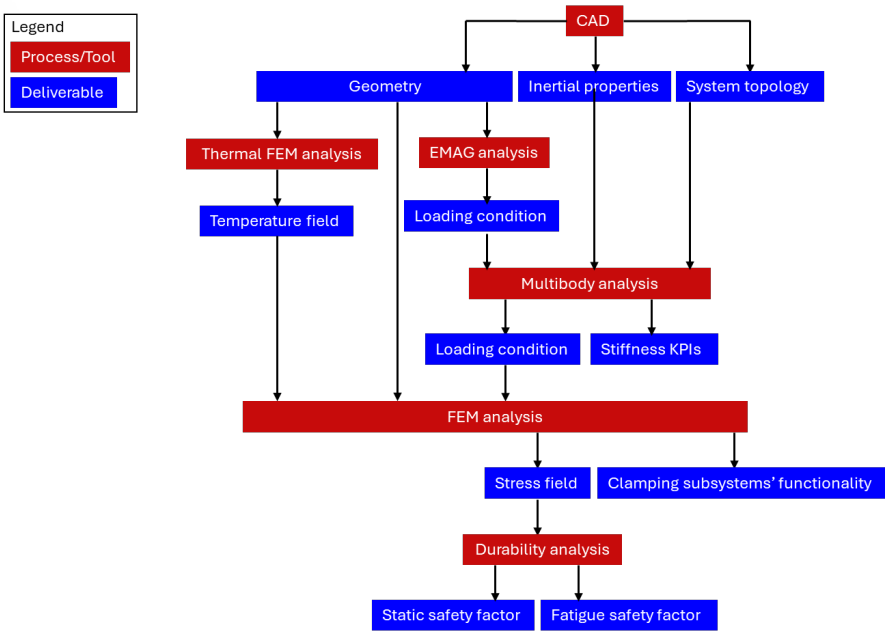

Figure 2: Modelling remarks. E-motor's cover. CAE workflow

The same multibody model was used to feed the subsequent analyses. The models used for specific analyses are described in the following paragraphs.

The EMAG simulations singled out the e-motor power and torque characteristics, which in turn were used to carry the structural FEM analyses. More specifically, the EMAG simulations are useful to define the electromagnetic force acting on stator teeth, over a complete mechanical revolution of the rotor parts.

In addition to the forces exchanged between rotating and static parts, the EMAG simulations identifies the torque ripple generated over the complete range.

The EMAG simulations were carried out at different speeds, representing design working conditions. The power/torque characteristics were computed as functions of the electric machine shaft's rotation angle.

EMAG analysis

The EMAG analyses were divided into parallel activities:

- 2D lumped parameters simulations;
- 2D & 3D FEA simulations.

The first set of simulations were used to identify:

- Short Circuit & No-load conditions;
- The peak and continuous performances;
- Id-Iq current maps;

The second set of simulations were used to identify:

- Permanent Magnets demagnetization;
- Stator teeth electromagnetic force (radial and tangential);
- Torque ripple;
- Cogging torque.

In order to calibrates virtual models, specific on-bench tests were implemented on a first set of e-motor prototypes.

All the active parts were fully modelled in both simulation environments, to be compliant with the actual e-motor prototypes characteristics, both dimensional and physical ones.

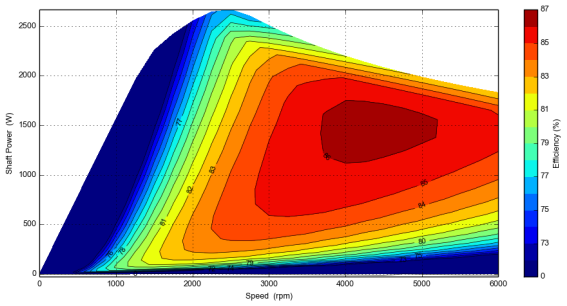

(a)

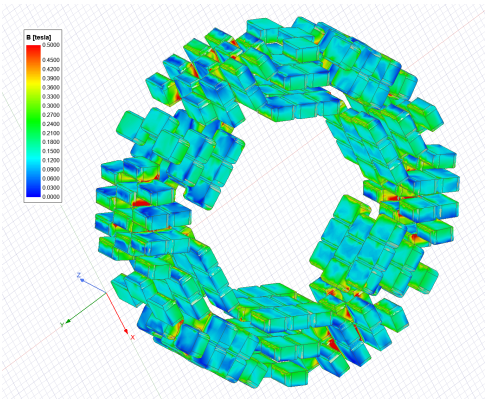

(b)

Figure 3: Modelling remarks. EMAG analysis. (a) e-Motor Efficiency Map, (b) Virtual Simulation of Permanent Magnets demagnetization

CFD analysis

This model's target was to provide the temperature field at the free surfaces of the bodies included in the system to be analysed.

Stationary conditions were assumed, simulating the reference working conditions prescribed by the project's specs, thus matching the EMAG modelling campaign's scenarios (see below)

Thermal analysis

This model's target was to provide the temperature field in the bodies included in the system to be analysed.

The following figure shows the bodies included in the model.

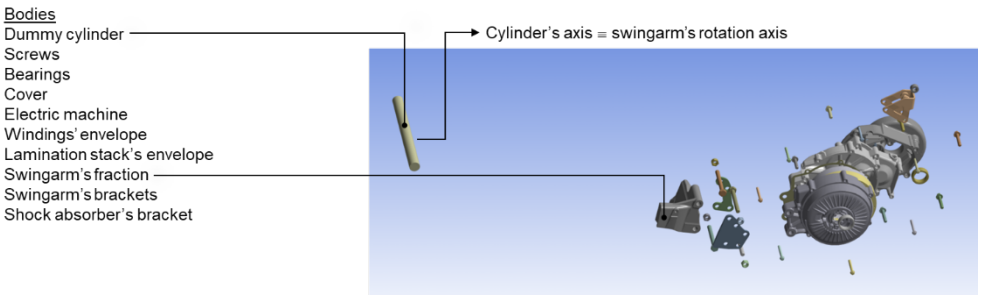

Figure 4: Modelling remarks. Thermal analysis. Bodies included in the model.

The dummy cylinder was used as a reference to apply a boundary condition to the modal used for the structural analysis, which had the same mesh as the one used for thermal analysis.

The stator's windings were modelled with a dummy body whose external surface coincides with the windings envelope's.

Thermal continuity was assumed at the interfaces between adjacent bodies.

The involved bodies' thermal properties were assumed not to depend on the temperature.

Steady-state conditions were assumed.

Multibody analysis

This model's target was to provide the time-histories of the loads acting on the bodies whose structural soundness was to be analysed.

The following figure shows the rigid bodies included in the model.

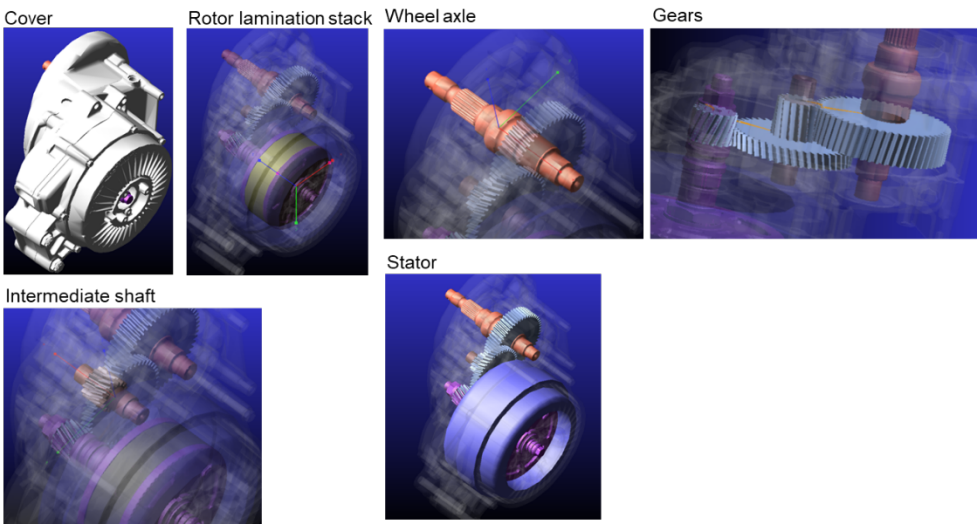

Figure 5: Modelling remarks. Multibody model. Rigid bodies.

The stator's windings were modelled with a dummy body whose external surface coincide with the windings envelope's. A dummy density was assigned to this bodies, assuming a 70% filling fraction for the envelope's volume.

The wheel axle was connected to a dummy rigid body whose inertia tensor's only non-zero element is the moment, called *I*, around the wheel axle's rotation axis.

The following quantities were defined.

M ≡ vehicle+rider mass

R ≡ rear wheel radius

t ≡ electric machine/wheel axle transmission ratio

s ≡ electric machine angular velocity

v ≡ vehicle speed

No rear tire slip was assumed.

I was computed so that the dummy rigid body has the same kinetic energy as the vehicle/rider system.

$$\frac{1}{2}Mv^2 = \frac{1}{2}I(st)^2$$

Thus,

$$I = MR^2$$

A flexible was included in the model, representing the electric machine shaft's subsystem, including the shaft proper, the plates which clamp the rotor's lamination stack, and all the components to keep those plates in place.

This body's flexibility properties were computed via FEM with the Craig-Bampton method [1]. The following figure shows the flexible body.

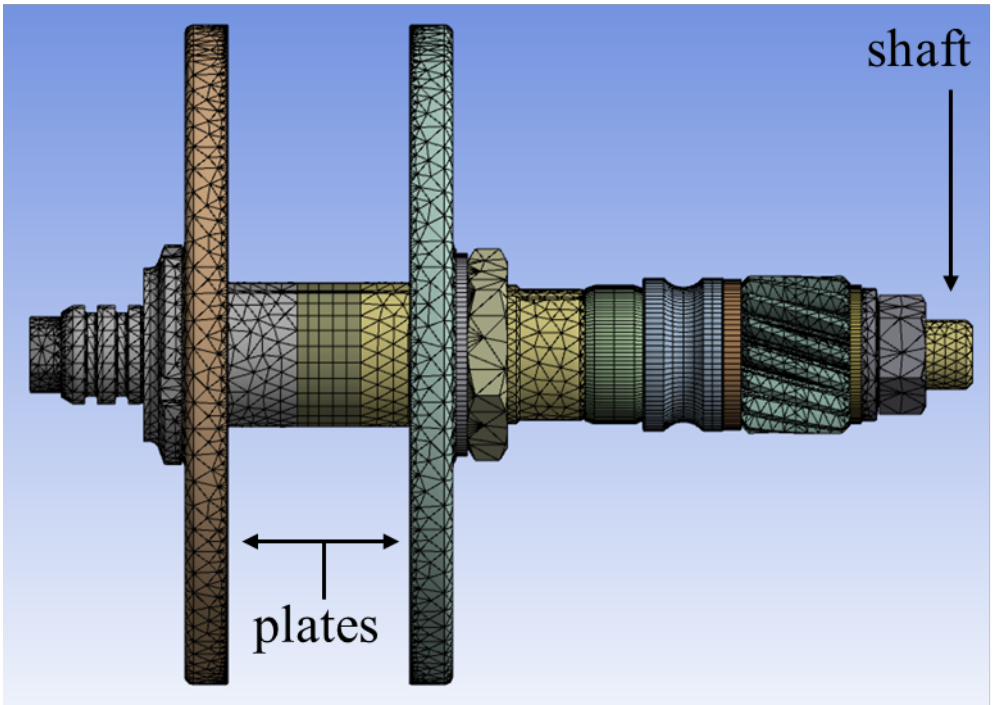

Figure 6: Modelling remarks. Multibody model. Flexible body.

Structural continuity was assumed at the plates/lamination stack interfaces, shown in the following figure.

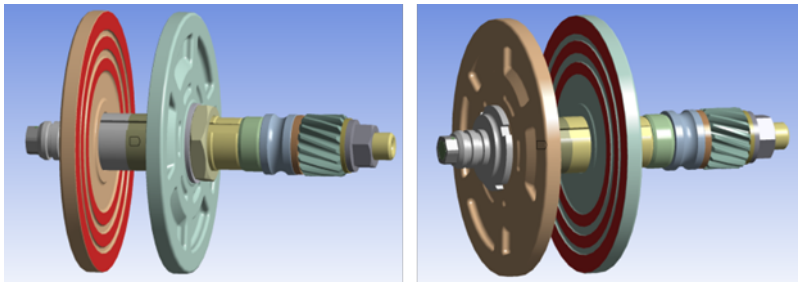

Figure 7: Modelling remarks. Multibody model. Plates/stack interfaces.

The shafts included in the model were supported by kinematic constraints.

The gears were coupled with a pseudo-viscoelastic force, based on a kind of penalty approach. The force's pseudo-elastic component depends on the relative displacement between the conjugate gears as shown in the following figure.

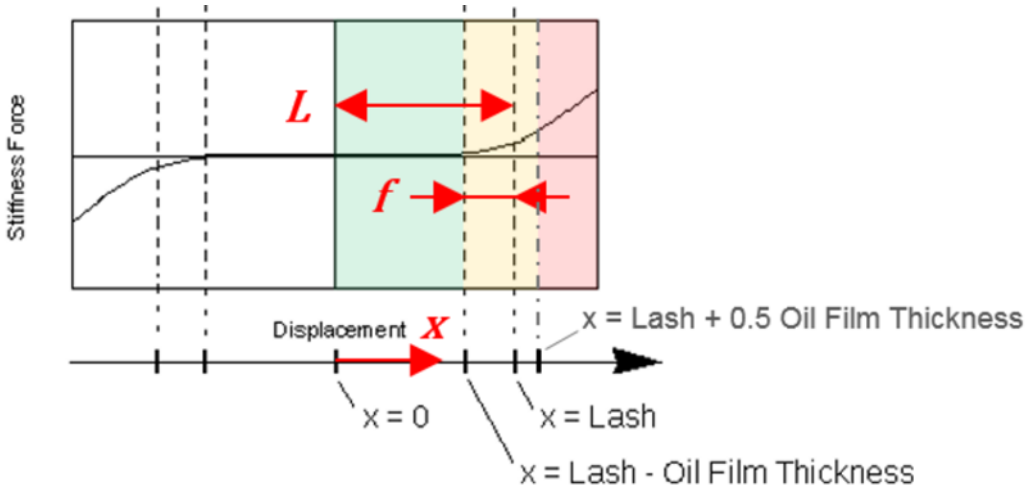

Figure 8: Modelling remarks. Multibody model. Gear force's pseudo-elastic component.

The pseudo-viscous component's details are omitted here for brevity's sake.

The e-motor max torque condition was simulated.

Structural FEM analysis

These models' targets were the following:

- provide the stress field to be input in the following durability analysis;
- assess the soundness of the friction couplings.

Cover analysis

The model included the bodies shown in Figure 4: The swingarm's fraction, the swingarm's bracket and the shock absorber's brackets were included to describe the local flexibilities at the cover's external connections, in order to avoid spurious regions in the computed stress field.

The swingarm connects the powertrain to the vehicle frame, as shown in the following figure.

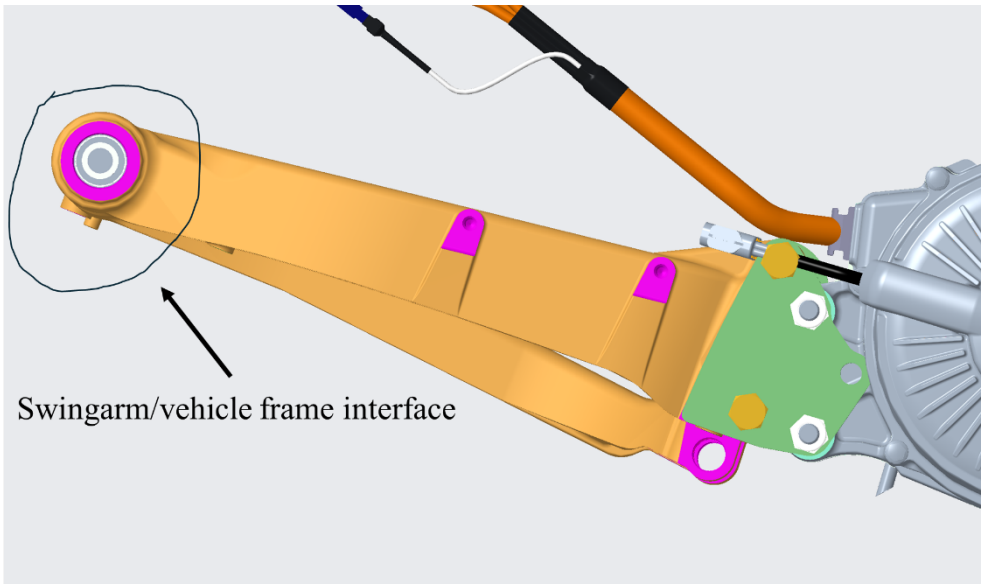

Figure 9: Modelling remarks. Structural FEM analysis. Cover analysis, Swingarm.

Negligible relative displacements between the laminations were assumed. Thus, the whole stack was simulated with a single flexible body.

The screws' threaded connections were not modelled: structural continuity was assumed.

Nonlinear frictional contact conditions were set at all the other interfaces between adjacent bodies.

No material nonlinearities were taken into account. Possible local plasticizations were taken into account during the durability analysis.

Shaft's subsystem analysis

The following figure shows the bodies included in the model.

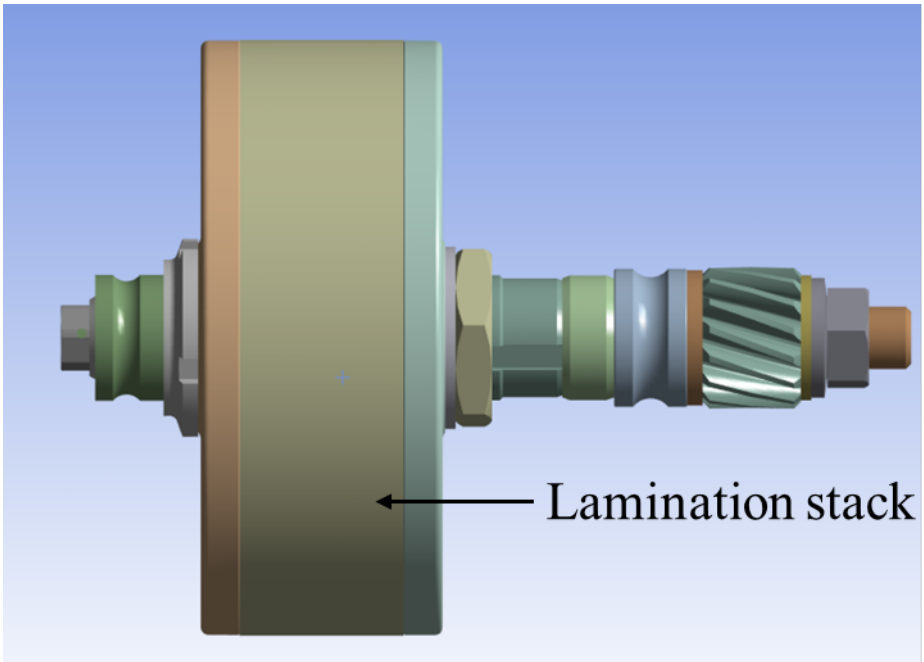

Figure 10: Modelling remarks. Structural FEM analysis. Shaft's subsystem analysis. Bodies included in the model.

Negligible relative displacements between the laminations were assumed. Thus, the whole stack was simulated with a single flexible body.

The threaded connections were not modelled: structural continuity was assumed.

Nonlinear frictional contact conditions were set at all the other interfaces between adjacent bodies.

Durability analysis

These models' target was to compute the durability safety factors, to be compared with allowable limits according to Piaggio's standards.

The Uniform Material Law method [2] was used when test data were not available, as for the materials' fatigue properties.

The fatigue cycles' mean stress and mean strain effects were taken into account via the Goodman and Smith-Watson-Topper methods.

The effect of the relative stress gradient on the fatigue performance was taken into account according to the FKM guidelines [3].

Cover analysis

The endurance limits' variations with the temperature were taken into account singling out temperature bands and assigning different fatigue limits to the relevant cover regions. The following figure shows the temperature bands and the corresponding endurance limits which were taken into account.

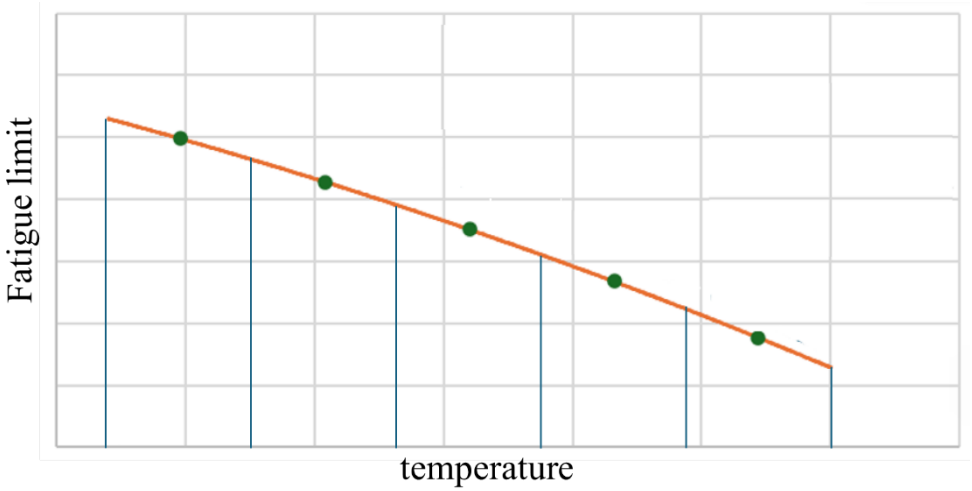

Figure 11: Modelling remarks. Durability analysis. Motor cover. Fatigue limit/temperature function.

The strain-life method was used.

The Neuber correction [4] was used to describe possible plastic phenomena affecting the materials.

Shaft's subsystem analysis

The stress-life method was used.

3. Initial and boundary conditions

EMAG analysis

In order to reduce the simulation time the complete model was reduced taking advantage of periodicity of the e-Motor, therefore a single pole (60° mechanical) can be simulated to evaluate the complete e-Motor performance (see also Figure 12:).

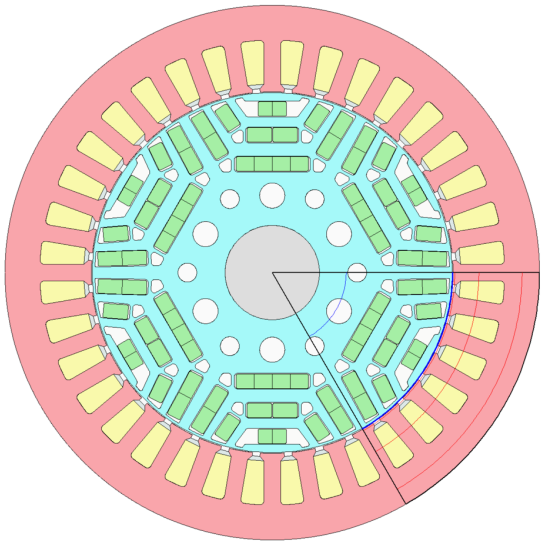

Figure 12: Initial and boundary conditions. EMAG analysis. eMotor simmetry for a reduced model simulation

CFD analysis

A steady-state condition was modelled, simulating fluid approaching the systems with constant velocity, as shown in the following figure:

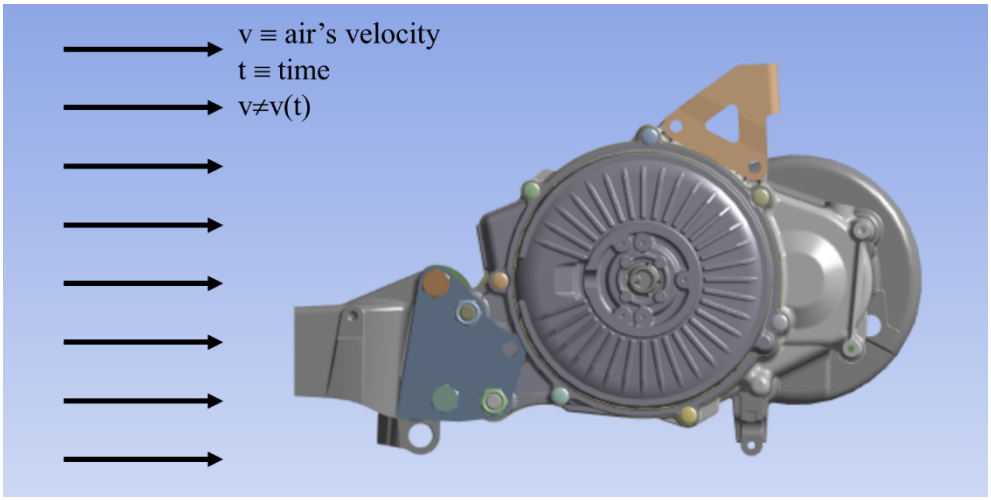

Figure 13: Initial and boundary conditions. CFD analysis. External flow

Three different e-motor speed were simulated. They are the design speeds; among them there is the max torque condition.

Using kinematic constraints, the vehicle speed corresponding to the motor design speeds were computed. The vehicle speeds were used to build the boundary condition shown in Figure 13: .

Thermal FEM analysis

The temperature field on all the bodies' surfaces were imported from the CFD analyses, for each e-motor speed.

The following figure shows one those fields, highlighting the hot region at the stator's windings.

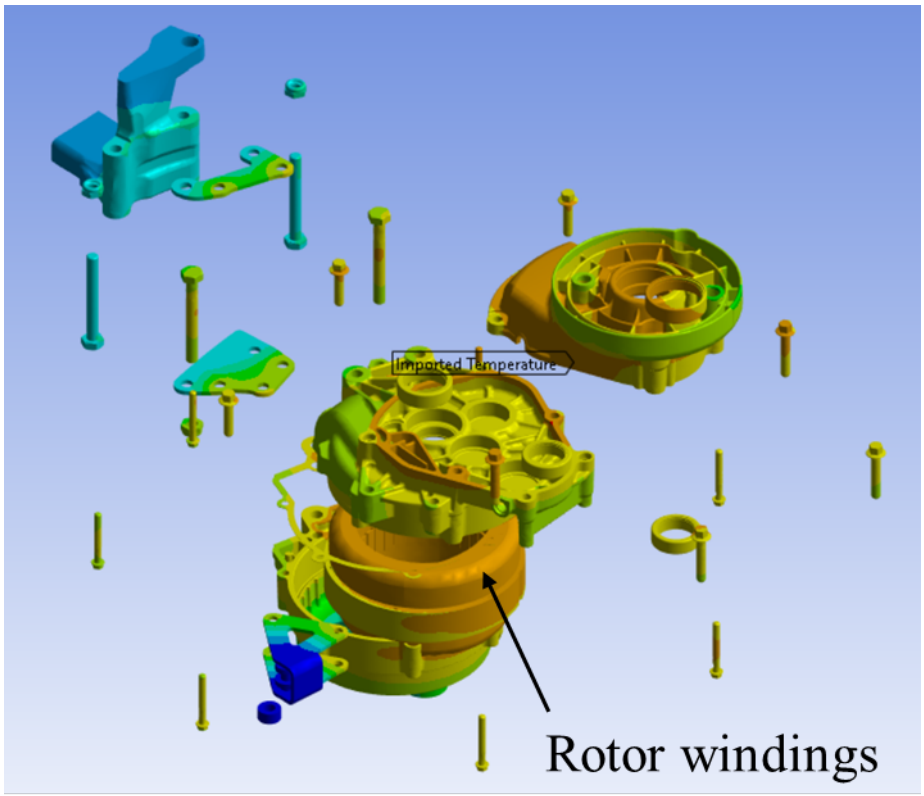

Figure 14: Initial and boundary conditions. Thermal FEM analysis. Imported temperature field.

Multibody analysis

An action-reaction torque was applied to the electric machine's rotor and stator, as shown in the following figure.

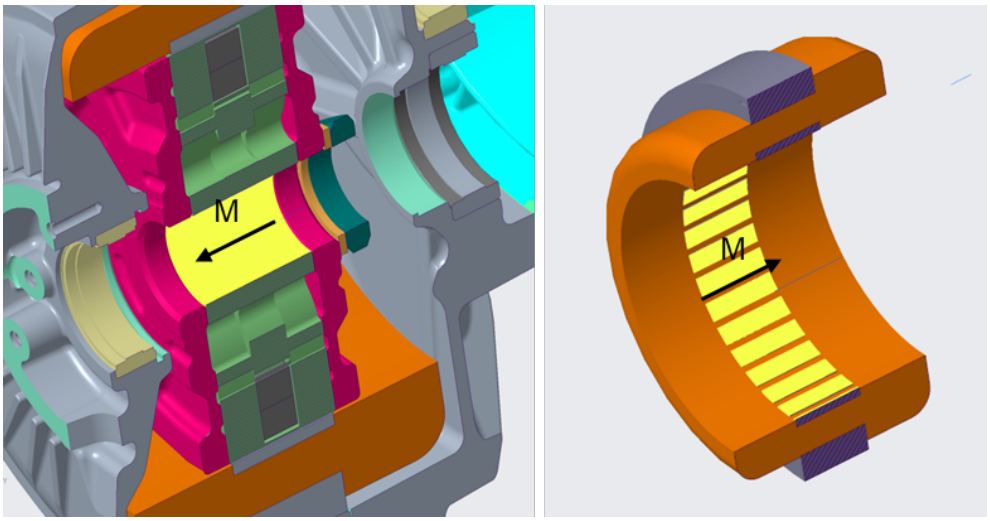

Figure 15: Initial and boundary conditions. Multibody analysis. Action-reaction torque.

Let θ be the e-motor's shaft rotation angle. The M(θ) function was computed via the EMAG analysis. The following figure shows the M(θ) function.

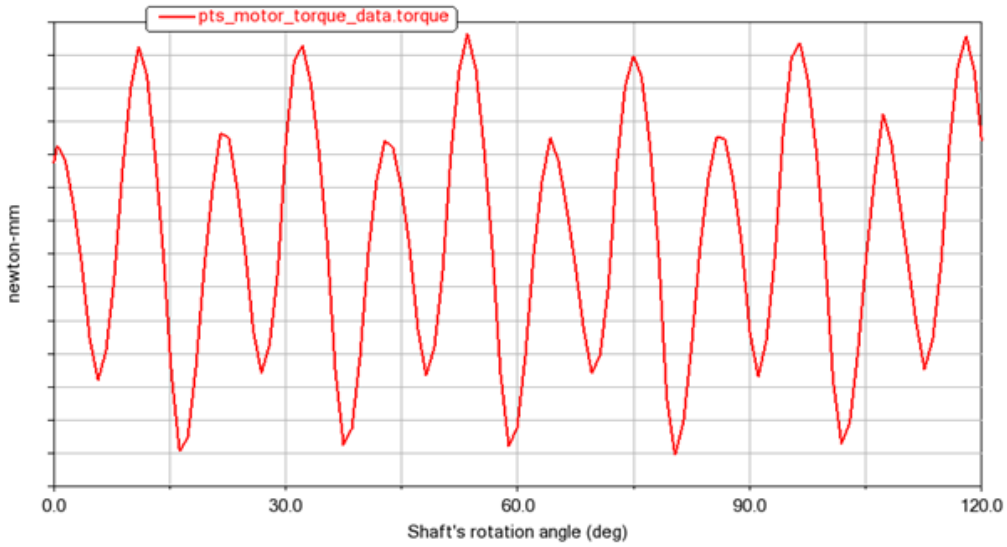

Figure 16: Initial and boundary conditions. Multibody analysis. Motor torque.

The following quantities were defined

ω ≡ electric machine shaft/wheel axle transmission ratio

$$\bar{M} \equiv \frac{3}{2\pi}\int_0^{\frac{2\pi}{3}} M d\theta$$

A constant torque, whose module is $M\omega$, was applied to the dummy body representing the vehicle, thus obtaining stationary conditions.

Structural FEM analysis

Cover analysis

The mechanical loads coming from the multibody model correspond to the max torque condition. This set of boundary conditions was coupled with each thermal condition, as shown in the following table

Full boundary condition set id	**Mechanical loads' working condition**	**Thermal condition**
M1	Max torque	e-motor design speed 1
M2	Max torque	e-motor design speed 2
M3	Max torque	e-motor design speed 3

Table 1: Initial and boundary conditions. Structural FEM analysis. Cover analysis. Combined boundary condition.

The assumption behind the way the mechanical and thermal loads were combined is that the e-motor can experience the max torque mechanical condition at every working temperature, due to its thermal inertia.

The shafts are supported on bearings. The corresponding loads were applied at the cover's interfaces with the bearings, with a sine spatial distribution, as shown in the following figure.

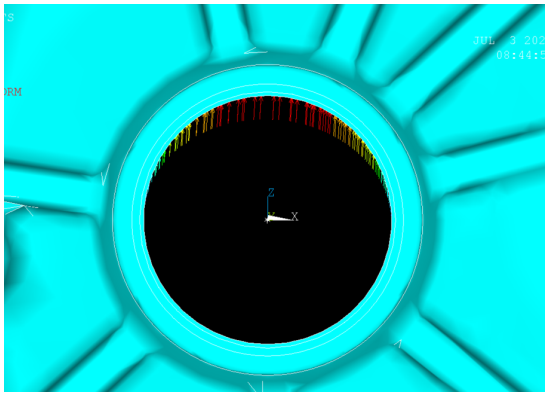

Figure 17: Initial and boundary conditions. Structural FEM analysis. Cover analysis. Bearing loads.

For each Table 1: row, N loading conditions were singled out, corresponding to the extrema of each mechanical load component acting on the cover, as shown in the following figure for a bearing load's component.

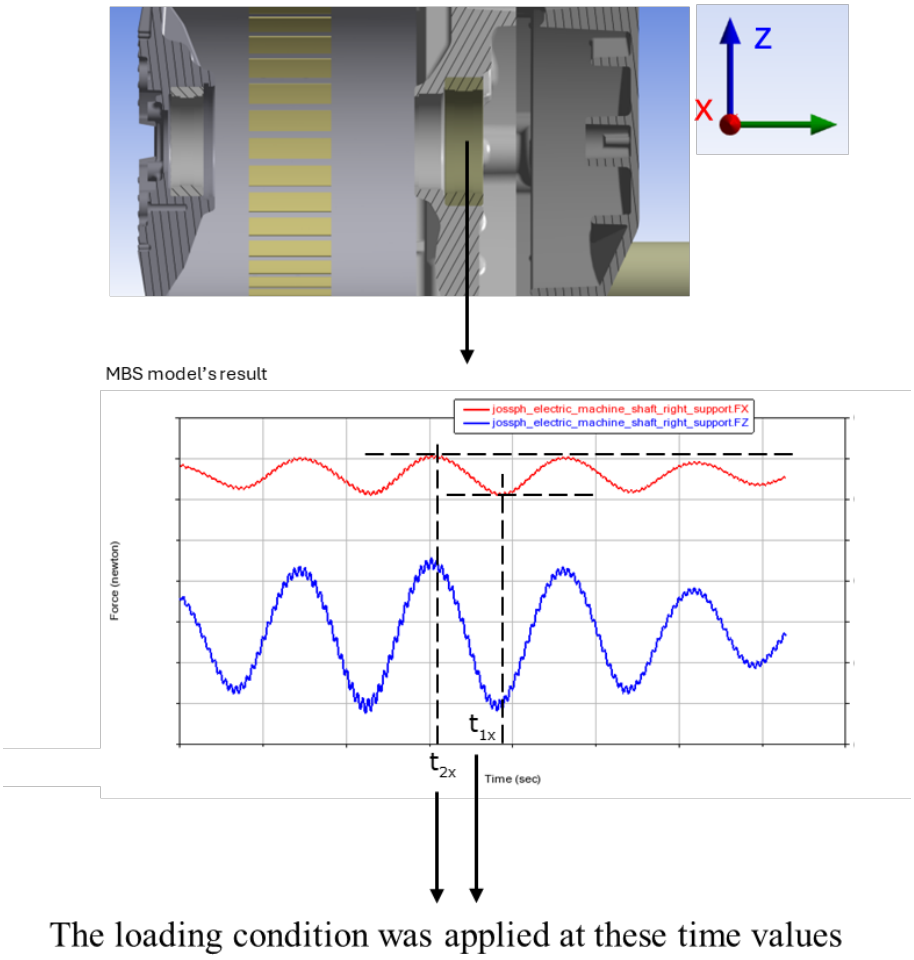

Figure 18: Initial and boundary conditions. Structural FEM analysis. Cover analysis. Loading conditions.

The process was repeated for each load component and for each interface, obtaining N time values. In addition to the dynamic ones, static mechanical loads were applied. The complete loading sequence is shown in the following table.

Load step index	Applied loads
1	• Screws' preload • Interference fit loads at bearings' interfaces
2	• Screws' preload • Interference fit loads at bearings' interfaces • Temperature field computed via FEM thermal analysis
3	• Screws' preload • Interference fit loads at bearings' interfaces • Temperature field computed via FEM thermal analysis • Time-varying load at time t_{1x} (Figure 18:
4	• Screws' preload • Interference fit loads at bearings' interfaces • Temperature field computed via FEM thermal analysis • Time-varying load at time t_{2x}
…	…

Table 2: Initial and boundary conditions. Structural FEM analysis. Cover analysis. Load sequence.

The model was constrained at the front e-motor/vehicle frame interface as shown in the following figure.

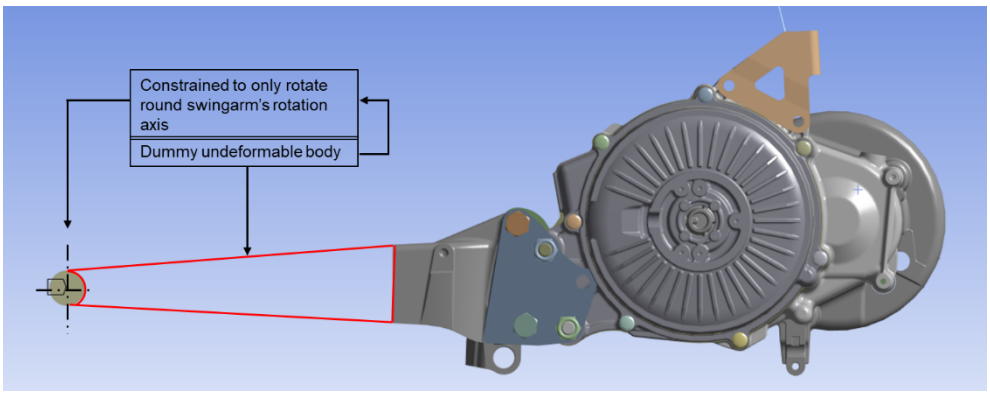

Figure 19: Initial and boundary conditions. Structural FEM analysis. Cover analysis. Boundary condition at the front e-motor/vehicle frame interface.

The model was constrained at the rear e-motor/vehicle frame interface as shown in the following figure.

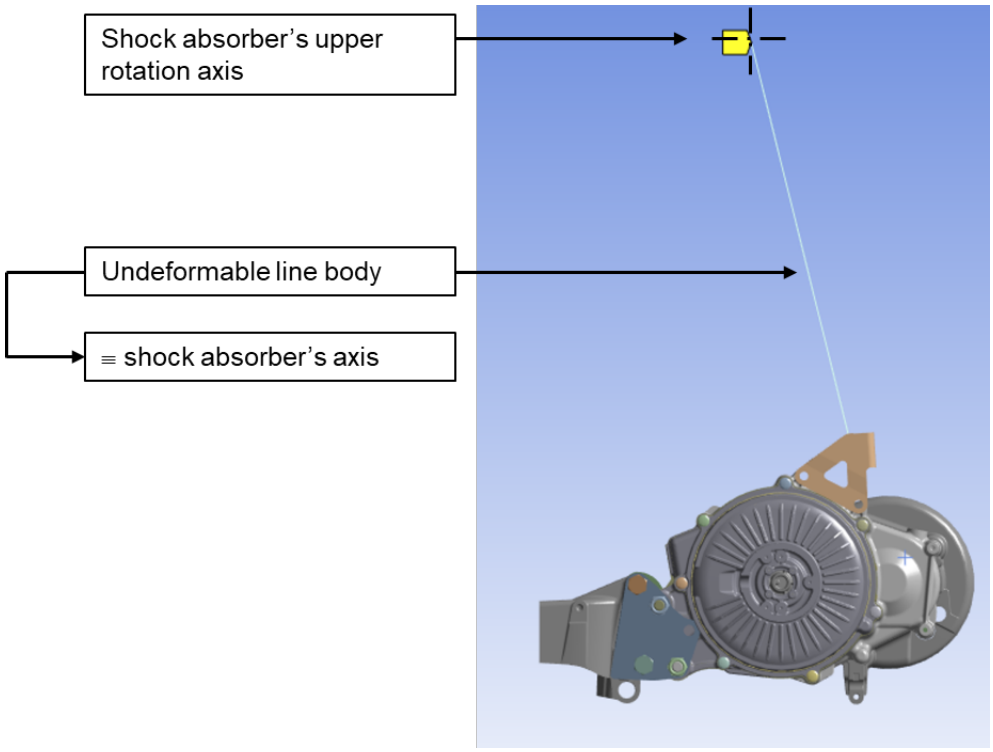

Figure 20: Initial and boundary conditions. Structural FEM analysis. Cover analysis. Boundary condition at the rear e-motor/vehicle frame interface.

Shaft's subsystem analysis

The load channels are shown in the following figure.

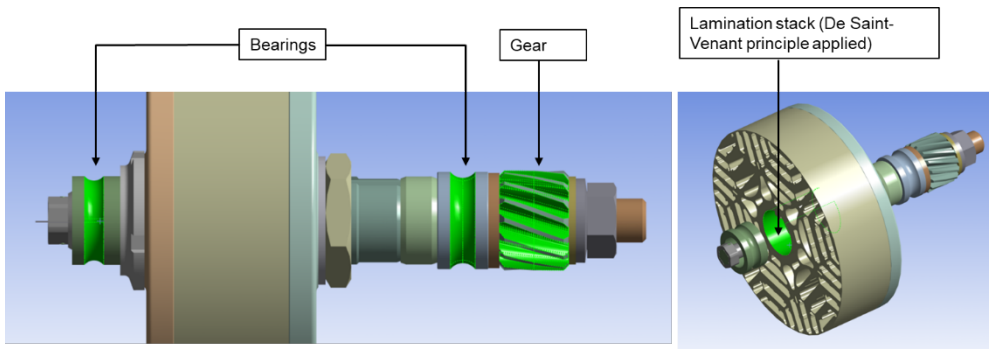

Figure 21: Initial and boundary conditions. Structural FEM analysis. Shaft's subsystem analysis. Load channels.

The torque acting on the lamination stack was applied to the shown surface leveraging the De Saint-Venant principle, since the lamination was not among the bodies where the stress field had to computed.

A mass force field was applied based on the angular velocity and angular acceleration time-histories computed with the multibody model. Thus, dynamic equilibrium conditions could be simulated using an FEM static solver.

The load conditions were chosen with the method shown in Figure 18: , applied to each of the load channels shown in Figure 21: and to the mass force fields.

Durability analysis

Cover analysis

The fatigue cycle was defined by steps 2÷N shown in Table 2:

Shaft's subsystem analysis

The fatigue cycle was defined by the time values singled out with the method shown in Figure 18:

4. Results

EMAG analysis

After a complete set of simulation, the main characteristics of the e-Motor were identified and transferred to the structural and thermal FEM solver (see also Figure 22:).

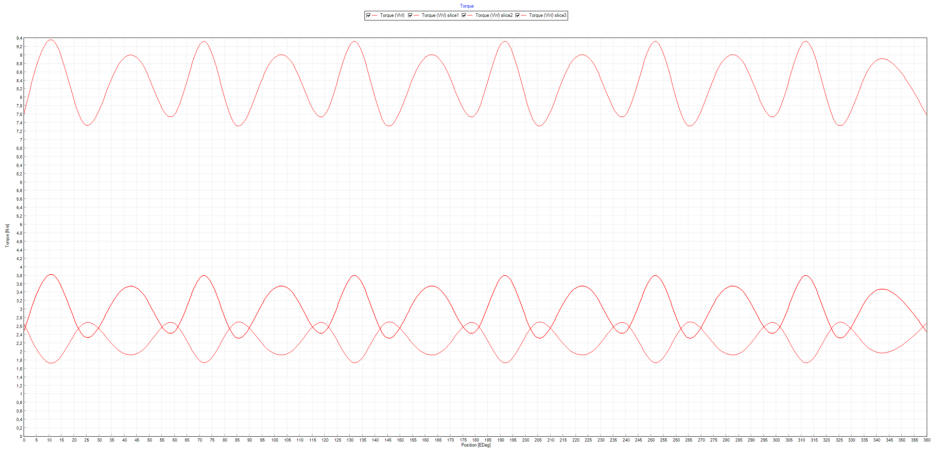

Figure 22: Results. EMAG analysis. Torque ripple evaluation @2500 rpm

All terms of losses were identified and used to feed also the CFD simulations (see also Figure 23:).

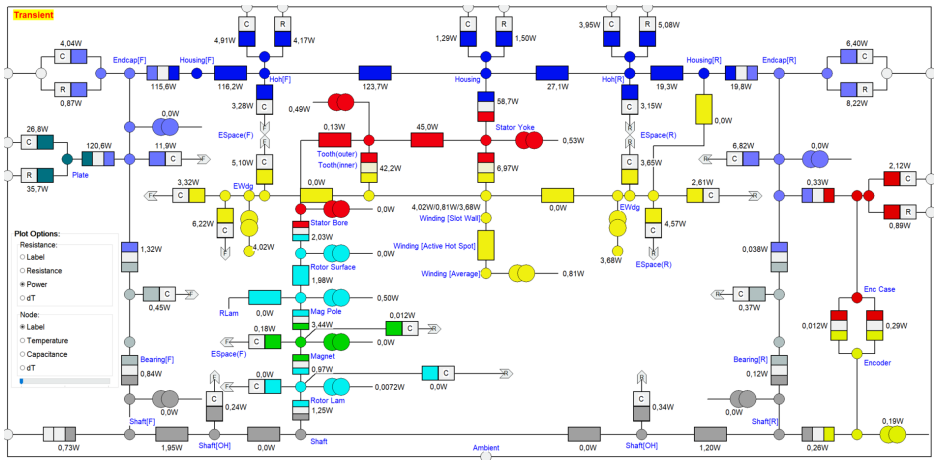

Figure 23: *Results. EMAG analysis. Thermal net with the details about the complete terms of loss*

Structural FEM analysis

Cover analysis

The following figure shows the cover/lamination stack interface surface, called *S*.

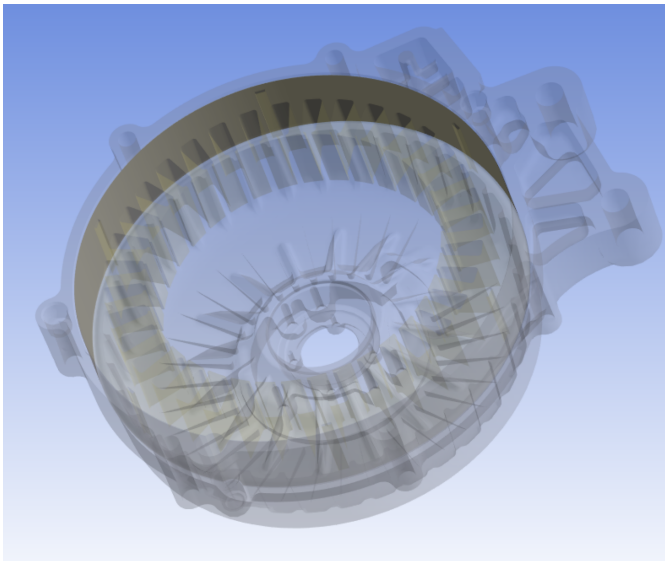

Figure 24: Results. Structural FEM analysis. Cover analysis.

The following quantities were defined.

A ≡ area of S

P(x,y,z) ≡ generic point on S

p(x,y,z) ≡ contact pressure at P

τ(x,y,z) ≡ shear stress at p, on a plane tangent to S

f ≡ cover/lamination stack friction coefficient

$$\varsigma(x,y,z) \equiv \begin{cases} 1\ if\ p = 0 \\ 2\ if\ \dfrac{\tau}{p} > f \\ 2\ if\ \dfrac{\tau}{p} < f \end{cases}$$

$$\eta \equiv \frac{1}{A}\int_S \varsigma(x,y,z)dS$$

$$\psi \equiv \max_{x,y,z}\{\varsigma(x,y,z)\}$$

η was used as a functionality index of the interference fit coupling between the lamination stack and the cover; the higher, the better. It was used to single out the most severe loading condition from this standpoint.

ψ was used to qualify the interference fit coupling between the lamination stack and the cover in the presence of dynamic loads: it must be lower than 3 to avoid rigid body motions of the lamination stack. Values lower than 3 are acceptable while tightening threaded elements.

The following figure shows the values of η and ψ, for the most severe boundary condition set among those listed in Table 1:

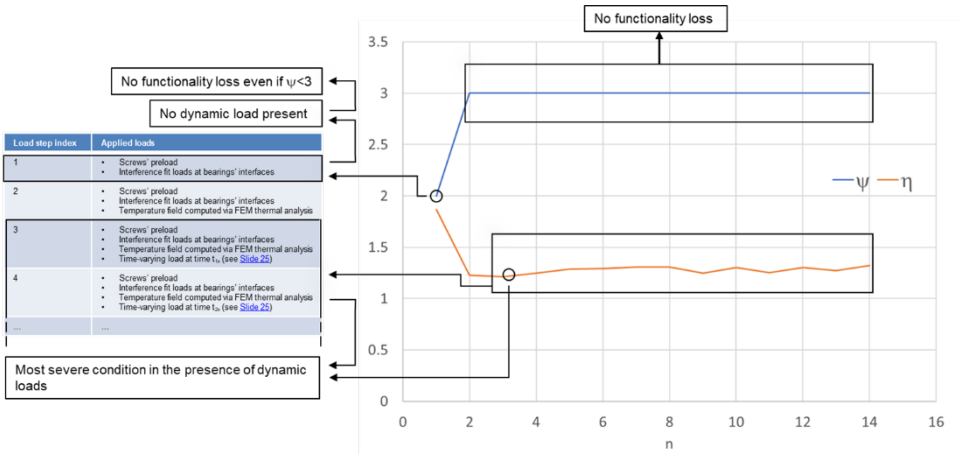

Figure 25: Results. Structural FEM analysis. Cover analysis. Functionality assessment of the interference fit coupling between the cover and the lamination stack.

The following figure the map of ζ for the most severe condition singled out in Figure 25:

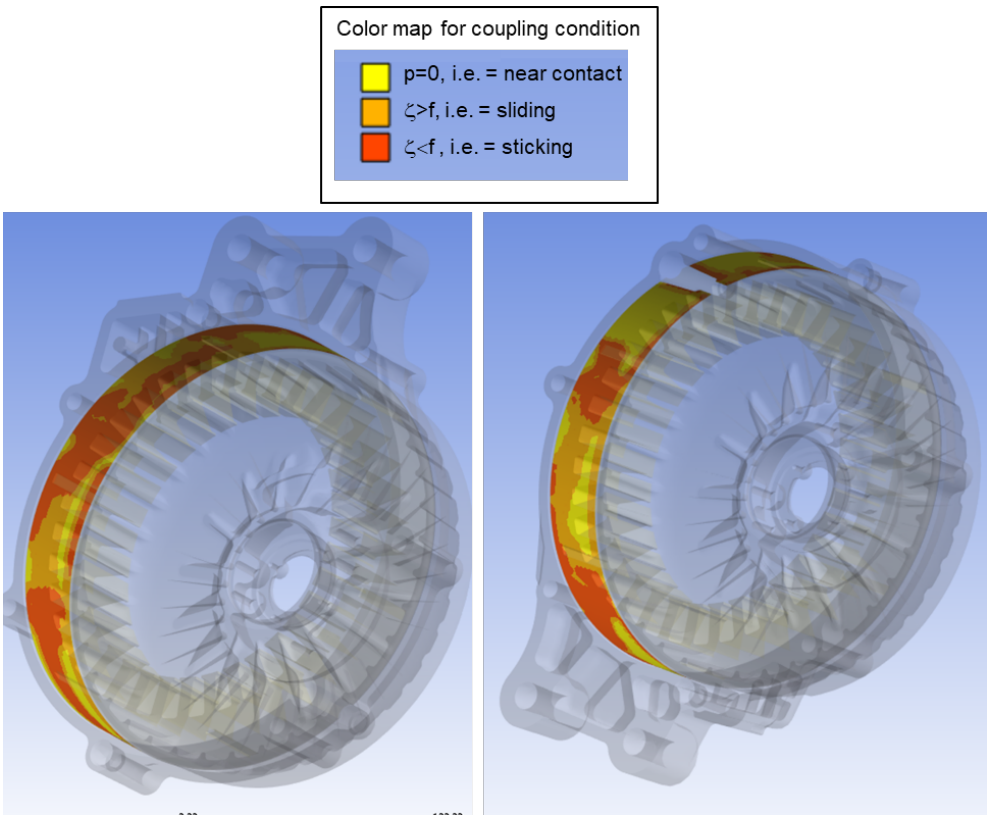

Figure 26: Results. Structural FEM analysis. Cover analysis. Map of the functionality index for the interference fit coupling between the cover and the lamination stack.

Shaft's subsystem analysis

The plates shown in Figure 7: are kept in place wrt the shaft with friction couplings. The whole subsystem is clamped with threaded elements. The following figure shows all the subsystem's friction couplings.

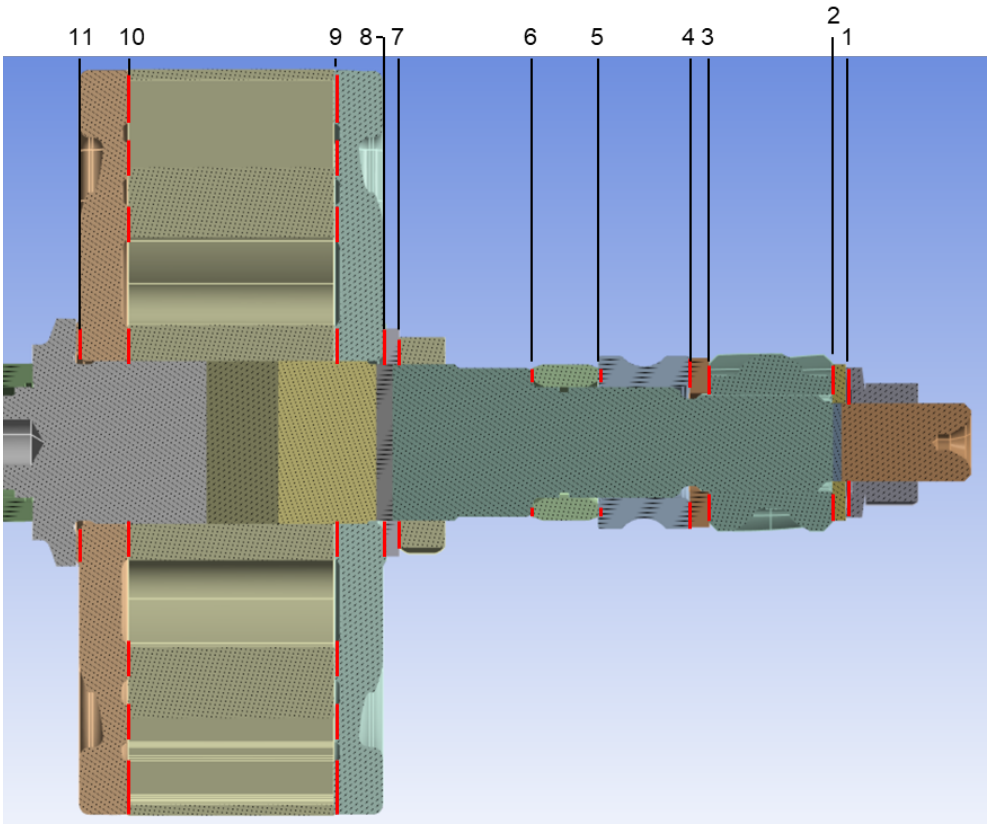

Figure 27: Results. Structural FEM analysis. Shaft's subsystem analysis. Friction couplings.

The η and ψ indexes (see cover analysis) were defined for the shaft's subsystem too, verifying the functionality of each of the interfaces shown in Figure 27: All the interfaces turned out to be functional (ψ=3); the following figure shown the map of η for interfaces #9 and #10 (see Figure 27:), which turned out to be associated with η's lowest value.

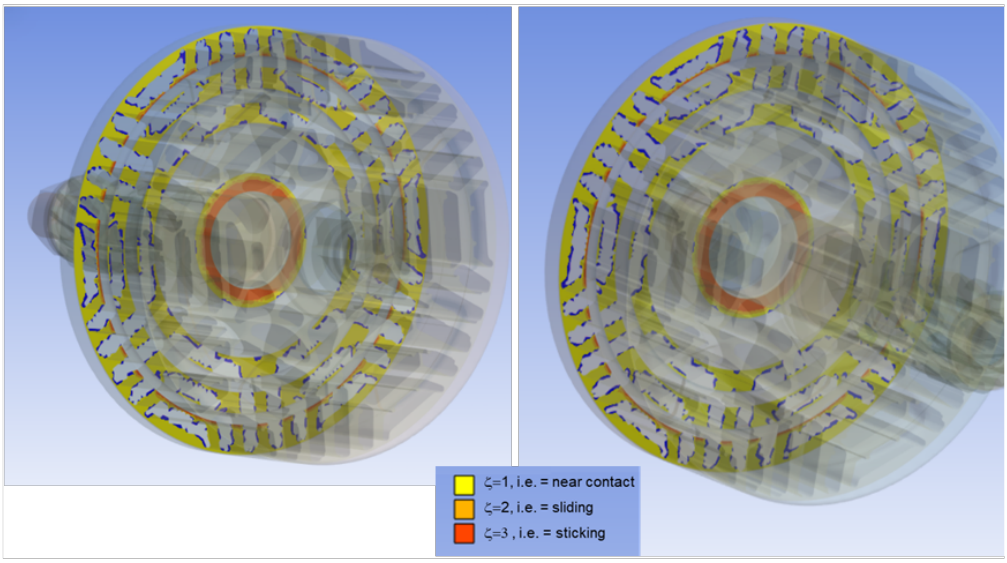

Figure 28: Results. Structural FEM analysis. Shaft's subsystem analysis. Friction couplings' functionality index.

Durability analysis

Cover analysis

The condition associated with the maximum e-motor design speed turned out to be most severe from a durability standpoint.

The cover consists of three bodies. The following figures show the maps of the fatigue safety factor for each body.

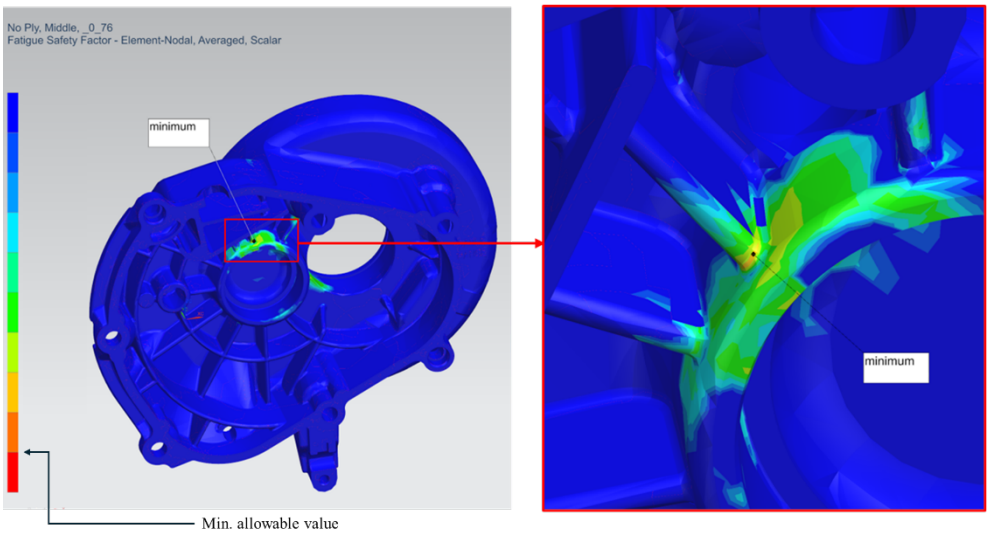

Figure 29: Results. Durability analysis. Cover analysis. Sub-cover #1. Map of the fatigue safety factor.

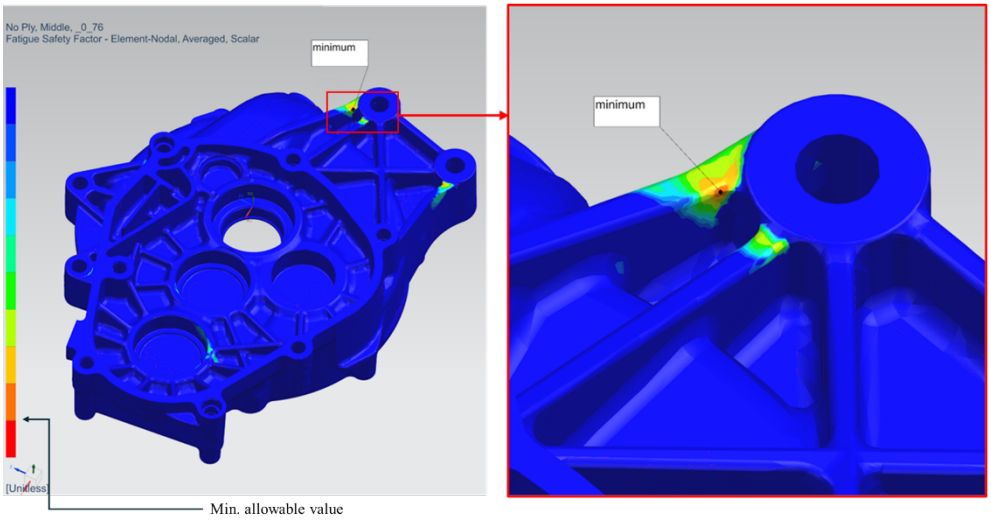

Figure 30: Results. Durability analysis. Cover analysis. Sub-cover #2. Map of the fatigue safety factor.

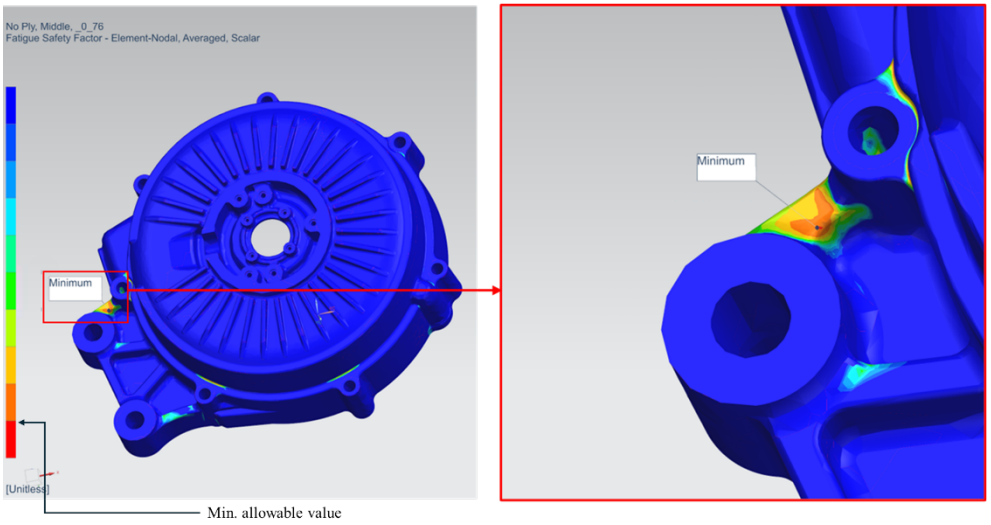

Figure 31: Results. Durability analysis. Cover analysis. Sub-cover #3. Map of the fatigue safety factor.

A reinforcement was devised for region highlighted in Figure 31: where the safety factor is lower than the allowable value. The following figure shows the reinforcement.

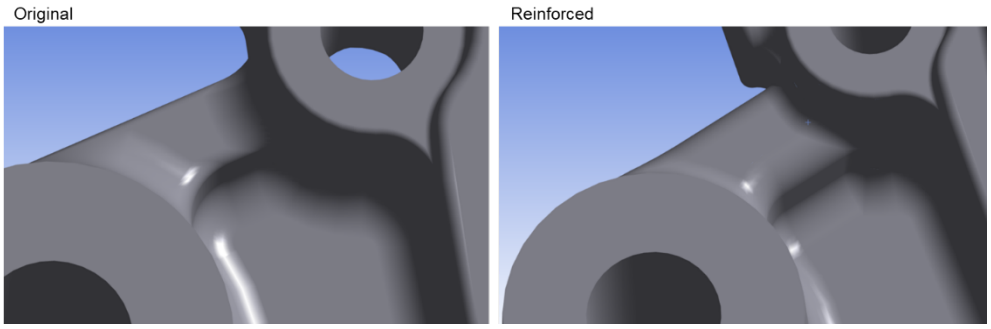

Figure 32: Results. Durability analysis. Cover analysis. Sub-cover #3. Reinforcement.

This design modification brought the safety factor's minimum value above the minimum allowable value, as shown in the following figure.

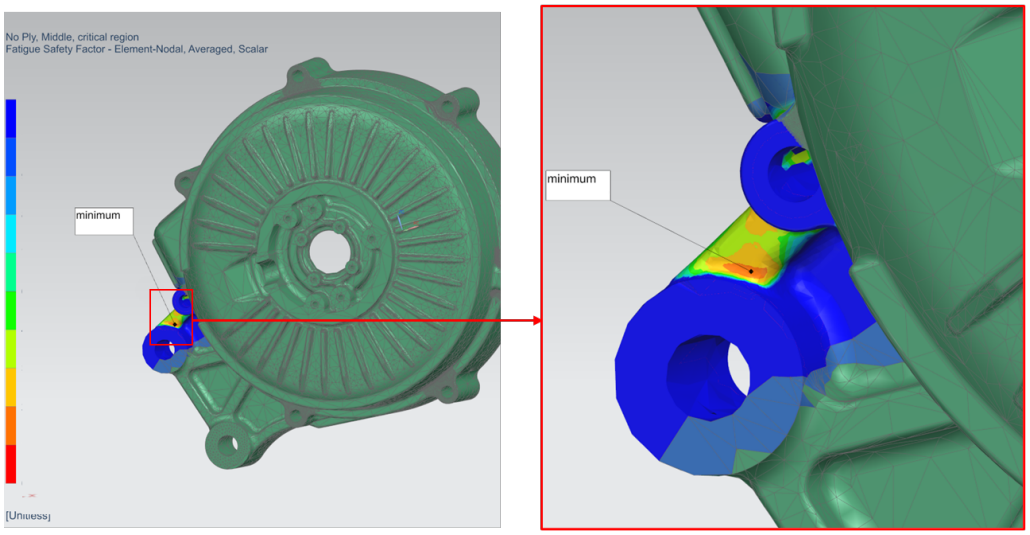

Figure 33: Results. Durability analysis. Cover analysis. Sub-cover #3. Modified geometry. Map of the fatigue safety factor.

Shaft's subsystem analysis

The following figures show the maps of the fatigue safety factor for the shaft.

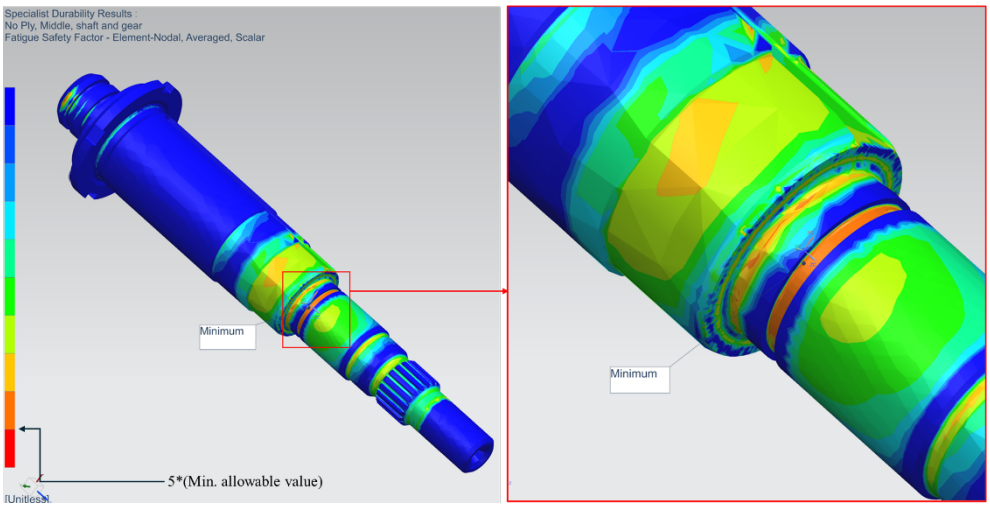

Figure 34: Results. Durability analysis. Shaft's subsystem analysis. Map of the fatigue safety factor.

Given the result shown in Figure 34: , no design modification was deemed necessary for the shaft.

5. Conclusions

A multidisciplinary CAE workflow allowed to assess the functionality of the e-motor's key subsystems and to devise dedicated design modifications when design criteria were not satisfied. Moreover, specific simulations and relative results substituted specific tests with e-motor and emotor+trasmission prototypes; in other words, virtual validation substitutes actual validation tests.

6. References

[1] R.R. Craig, M.C.C. Bampton - Coupling of substructures for dynamic analyses - AIAA Journal,vol. 6, n.7, 1968
[2] A. Baumel Jr., T. Seeger - Materials Data for Cyclic Loading, 1 - Elsevier Science Publishers, Amsterdam, 1990
[3] FKM Richtlinie - Rechnerischer Festigkeitsnachweis für Maschinenbauteile - 4., erweiterte Ausgabe 2002, VDMA Verlag
[4] Neuber, H. - Über Die Berücksichtigung Der Spannungskonzentration bei Festigkeitsberechnungen - Konstruktion, 20 (7), S. 245-251, 1968